Article

Comprehensive Understanding of the Planform Complexity of the Anastomosing River and the Dynamic Imprint of the River's Flow: Brahmaputra River in Bangladesh

Shiblu Sarker [1*], Tanni Sarker [2] and Sarder Udoy Raihan [3]

[1*] Bureau of Watershed Management and Modeling, St. Johns River Water Management District, Palatka, Florida, USA; shiblu.buet@gmail.com
[2] School of Planning, Design and Construction, Michigan State University, East Lansing, Michigan, USA; sarkerta@msu.edu
[3] Sub-Divisional Engineer, Bangladesh Water Development Board, Dhaka, Bangladesh; udoyraihan@gmail.com

Abstract: The Brahmaputra is one of the largest rivers in the world, ranking fifth in average discharge. As a result, it is heavily braided with various intricate paths in order to dissipate its huge energy. Although this river is normally classed as a braided river, it has recently been classified as an anastomosing river due to its multi-channel features over alluvial plains. Additionally, the Brahmaputra river's morphology is random in nature as a result of its high flow variability and bank erodibility. Its anastomosing planform changes in response to seasonal water and sediment waves, resulting in a morphology that is extremely complex. The purpose of this study is to examine the Brahmaputra river's anastomosing planform entropy as a measure of complexity, power spectral density as a measure of fluctuation and their relationship to the energy expenditure as an imprint of flow rate of river systems on alluvial landscapes.

Keywords: anastomosing; erodibility; planform; complexity; Fourier transform; power spectral density; sample entropy; approximate entropy

---

1. Introduction

Brahmaputra River is often characterized as Braided river, which usually is defined by a complex network of channels, branches and bars; as well as high sediment loads, significant variability of discharge and gradients [1,2]. Morphological processes such as erosion, deposition, channel migration and irregular planform creation associated with significant stream power variability are critical for understanding this particular type of river system [3–6]. These events occur repeatedly and frequently enough in braided systems to be measured over a short period of time. Numerous research have been conducted to better understand the form-process interactions of braided rivers. The majority of research include flume experiments [7–10], numerical modeling [11,12], satellite-based remote sensing products [13–18], and modern technology such as digital photogrammetry and laser altimetry [19–22].

This River system is one of the world's largest braided sand-bed river systems with it's fifth largest annual outflow in the world, giving it an ideal location to study morphological disorder [23–27]. In addition to that, this is an unique river system among large braided rivers in terms of its considerable inter-seasonal variability in flow-sediment load and morphological processes [26,28–30]. A series of large floods and major tectonic activity in this river system have resulted in a complex morphodynamic environment [26,31,32]. The banks of this large braided river system are heavily eroded, and the channel courses change frequently. These morphological changes have a tremendous impact on not just the riverine ecosystem, but also on the approximately 30 million people who live along its banks each year [33,34]. Understanding detailed morphodynamics is required to distinguish stable from unstable reaches and design natural and sustainable solutions.

The high variability of discharge and sediment load from the Brahmaputra basin in the Brahmaputra river system are responsible for significant erosion-deposition processes

Preprints (www.preprints.org) | NOT PEER-REVIEWED | Posted: 12 May 2022 doi:10.20944/preprints202205.0162.v1

[35–38] and also initiates complex network along with bar dynamics. To understand this complex morphodynamics, the spatio-temporal variability of planform and dynamic forcings should be investigated. Furthermore, it is also critical to investigate the effect of bar dynamics on the morphological changes associated with planform complexity. As a result, the article's focus is on the interpretations given by change detection through planform complexity and fluctuations via the following steps: a) detecting planform change using complex network theory; b) quantifying planform complexity using the notion of entropy; c) analyzing the planform's spatial disorderness using the entropy concept; d) computation of planform fluctuations using concept of power spectral density, and finally, e) understanding the planform's self-organized behavior and response to available stream flow using linear regression analysis.

2. Study Area

A huge portion of Brahmaputra river with appropriate geographical and temporal coverage is necessary to accomplish the purpose of this work. Therefore, we conduct the most portion of our research on the Brahmaputra river reach within Bangladesh (see figure 1).

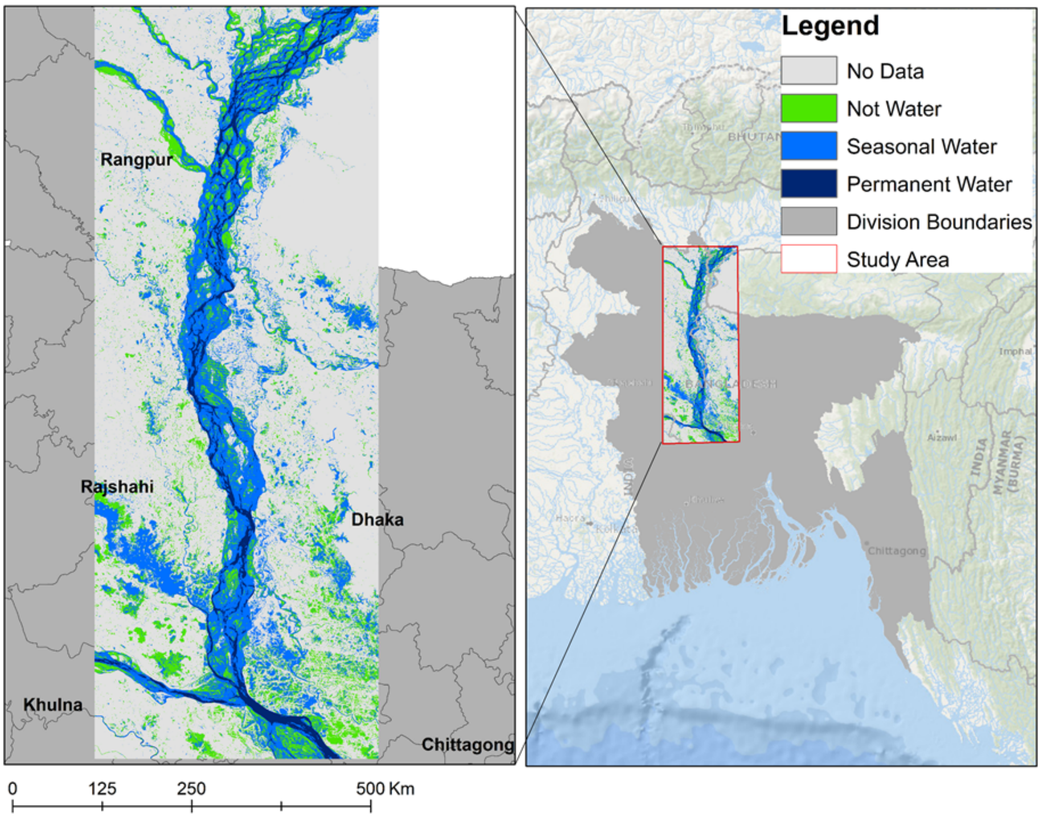

Figure 1. Study area of Brahmaputra River.

Several scholars have investigated the Brahmaputra in detail over a longer length of time. Our objective is to generate generic insights into the properties of planform complexity and dynamics of channel patterns that complement previous studies. As a result, we examine the Brahmaputra River from 1987 to 2020 using Landsat images within our study area (see figure 1). The Brahmaputra river has an average annual flood peak flow of 60000 m^3/s, with the monsoon flood typically occurring between July and August. The bankfull discharge volume is approximately 44000 m^3/s. The lowest discharges, approximately 5000 m^3/s, occur in January and February. The discharge is quite steady during this time period. Discharges steadily increase between March and June and gradually decrease between September and December [38,39].

Preprints (www.preprints.org) | NOT PEER-REVIEWED | Posted: 12 May 2022 doi:10.20944/preprints202205.0162.v1

3. Methods

3.1. Brahmaputra River employs the anastomosing river principle

Anastomosing rivers occur in alluvial plains. They are frequently discovered in low-energy local environments. Not only should anastomosing rivers be described by their channel vegetation, but also by their floodplain geomorphology and channel structure. The channels of anastomosing rivers may be straight, meandering or braided. Avulsions, or structures that redirect flow and create new channels in the floodplain, are frequently employed to build anastomosing rivers [40]. Simultaneous erosion of many floodplain channels takes place particularly when bypasses are constructed and older channel belt segments stay active for an extended period of time following bypassing. The first type of anastomosis affects the entire floodplain, whereas the second affects only a portion of it. Protracted anastomosis is generally caused by channel belt aggradation and/or channel capacity degradation as a result of in-channel deposition, both of which are facilitated by a low floodplain gradient [40]. Numerous other reasons are also climate-related such as catastrophic floods event and in-channel aeolian dunes or rapid base level rise. According to the criteria specified above, the Brahmaputra River is an anastomosing river, which provides an ideal setting for hypothesizing its planform as an anastomosing river planform [36] and thus applying complex network theory to gain a better understanding of physical processes occurring in its alluvial landscapes.

3.2. Channel Network Delineation

Using GEE, an image collection, or data stack, for yearly dry periods was created by combining all images intersecting the study area between October 1 and December 30 to create a cloud-free composite of scenes. This analysis used the tier 1 top of atmosphere (TOA) reflectance product to incorporate the entirety of the Landsat 5, 7, and 8 archives available for this area. The reflectance product is preferred over the TOA radiance product because it eliminates the exoplanetary effects associated with variable solar irradiance as a function of (1) solar zenith angles, (2) spectral band differences, and (3) Earth-Sun distance at various times of the year. ArcGIS 10.4.1 was used to delineate the Channel Network based on the annual seasonal and permanent water pathways.

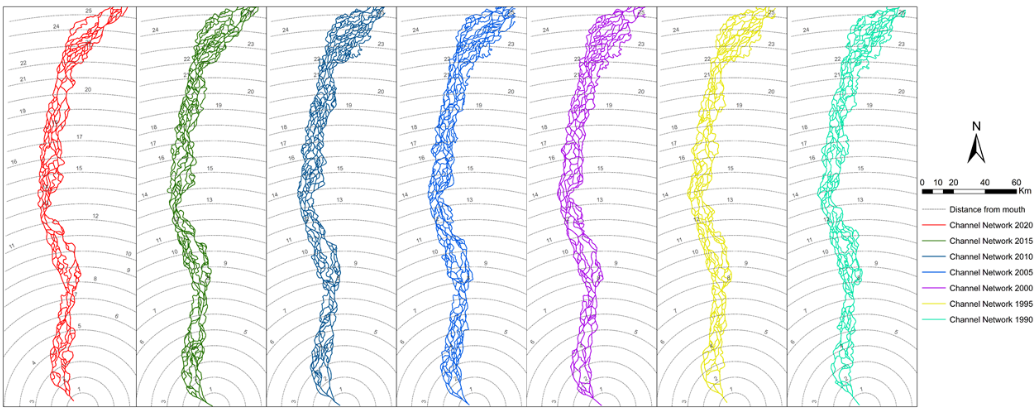

Figure 2. Delineation of the channel network for five selected years from 1990 to 2020, based on the dry season of Brahmaputra River.

3.3. Anastomosing function

In this study we have proposed a series entitled as Anastomosing function (*AF*) to capture one dimensional special arrangement of 2 dimensional complex network planform of Brahmaputra River. The concept of *AF* was developed employing a similar notion to that of a river basin's width function (see details in [35,41]). A river network's width function is a one-dimensional function that summarizes the river network's two-dimensional branching

Preprints (www.preprints.org) | NOT PEER-REVIEWED | Posted: 12 May 2022 doi:10.20944/preprints202205.0162.v1

structure [42]. Moreover, it displays the distribution of travel distances within the network as well as the probability distribution of travel durations under the assumption of constant flow velocity [42]. While, the width function represents the number of channelized pixels or number of crossed channels that have the same distance from the basin outlet where the distances are measured along the flow path [35,41], however, AF were computed the number of crossed channels as a function of the distance distance from the mouth of the Brahmaputra River rather than the outlet (see details in [36]). Furthermore, instead of measuring distance along the flow path (longest channel) we have adopted radial distance for simplicity of flow path from the mouth of the Brahmaputra River where it meets at the Ganges River. Mathematically Anastomosing function (AF) can be expressed as:

$$AF(d) = \#[Channelized\ I : d \leq R(I) \leq d + \delta d] \tag{1}$$

where $R(I)$ is the flow distance of channel intersection I from the mouth and δd is the scale of refinement. Usually the distance d is normalized by R and $AF(d)$ is normalized by the total number of channel intersection rendered it a density. For a given Anastomosing network topology, $AF(d)$ can be viewed as a stochastic process indexed by the distance d (as similar as width function [42]). Example of AF for five selected year were shown in figure 3a.

3.4. Discharge Data Collection

Yearly maximum discharge data of the Brahmaputra river for 1987-2020 spanning a 34 year period was collected from Bangladesh Water Development Board ($BWDB$) at Bahadurabad gauge station of Bangladesh (shown in figure 3b). BWDB serves as the national hydrological service provider organization of Bangladesh.

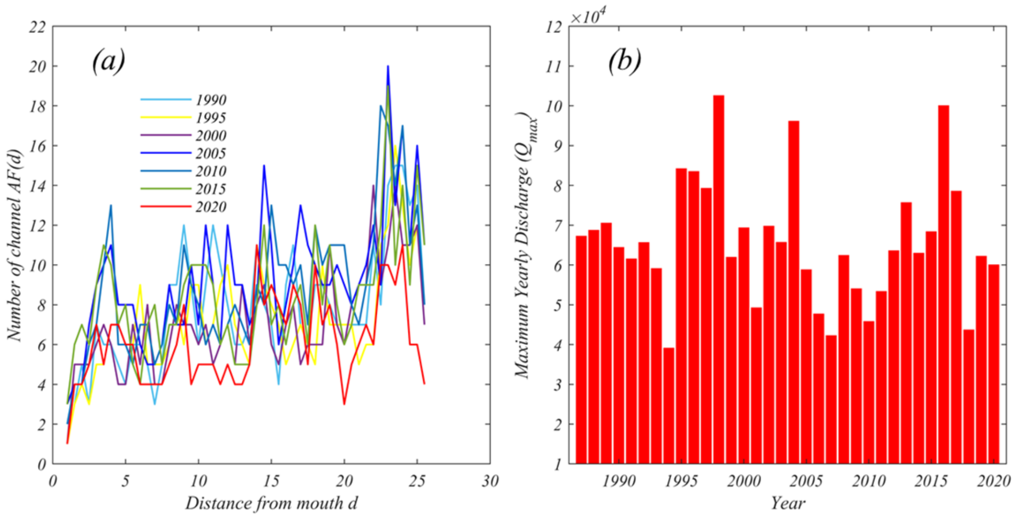

Figure 3. (a) Example of AF for five selected year and (b) Yearly maximum discharge data of the Brahmaputra river from 1987-2020.

3.5. Entropy

The entropy of a data series is a measure of its unpredictability. When moment statistics such as mean and variance are unable to differentiate between series, entropy can. In general, entropy quantifies the amount of information contained in a signal based on the probability of each signal value. In other words, entropy quantifies the degree of uncertainty associated with the occurrence of events across a space or time domain [43]. It can be expressed mathematically as

Preprints (www.preprints.org) | NOT PEER-REVIEWED | Posted: 12 May 2022 doi:10.20944/preprints202205.0162.v1

$$En = -\sum_{i=1}^{N} p[x(i)] \log p[x(i)] \tag{2}$$

where $p(x(i))$ is the probability of $x(i)$ and N is the sample size of the signal represented by a vector $S = x(1), x(2), \ldots\ x(N)$.

Approximate Entropy and Sample Entropy are two algorithms to determine the regularity of data series based upon the existence of patterns [44].

3.5.1. Approximate Entropy

While, approximate entropy is a form of entropy that calculation involves a large amount of data, Steve M. Pincus developed a method to deal with these limitations by modifying an exact regularity statistic [45]. Although it was initially developed for the study of medical data, its applications later expanded to other fields [35,45,46]. For example, we are interested to compute approximate entropy ($ApEn$) of a data series S containing N data values, $S = x(1), x(2), \ldots\ x(N)$. From this data, a series of vectors can be constructed as:

$$X(1) = x(1),\ x(2),\ \ldots\ x(m) \tag{3a}$$
$$X(2) = x(2),\ x(3),\ \ldots\ x(m+1) \tag{3b}$$
$$\ldots\ldots\ldots\ldots\ldots\ldots\ldots\ldots \tag{3c}$$
$$X(N-m+1) = x(N-m+1),\ x(N-m+2),\ \ldots\ x(N) \tag{3d}$$

The distance between two vectors $X(i)$ and $X(j)$ can be defined as the maximum difference in their respective corresponding elements.

$$d(X(i), X(j)) = \max_{k=1,2\ldots m} (|X(i+k-1), X(j+k-1)|) \tag{4}$$

where, $i = 1, 2, ..., N-m+1$ and $j = 1, 2, ..., N-m+1$ and N is the number of data points in the series. For each vector $X(i)$, a measure that describes the similarity between the vector $X(i)$ and all other vectors $X(j)\ j = 1, 2, \ldots, N-m+1,\ j \neq i$ can be constructed as:

$$C_i^m(r) = \frac{1}{(N-(m-1))} \sum_{j \neq i} \theta(r - d[X(i), X(j)]) \tag{5}$$

Where,

$$\theta(x) = \begin{cases} 1, & x \geq 0 \\ 0, & x < 0 \end{cases} \tag{6}$$

The symbol r specifies a filtering level and related to the standard deviation of the series. Finally, $ApEn$ can be calculated by the following equation:

$$ApEn(m, r) = \varnothing^m(r) - \varnothing^{m+1}(r) \tag{7}$$

Where,

$$\varnothing^m(r) = \frac{1}{(N-(m-1))} \sum_i ln[C_i^m(r)] \tag{8}$$

The application of approximate entropy ($ApEn$) on the $AF(d)$ data can be shown as the following flow chart (figure 4).

Preprints (www.preprints.org) | NOT PEER-REVIEWED | Posted: 12 May 2022 doi:10.20944/preprints202205.0162.v1

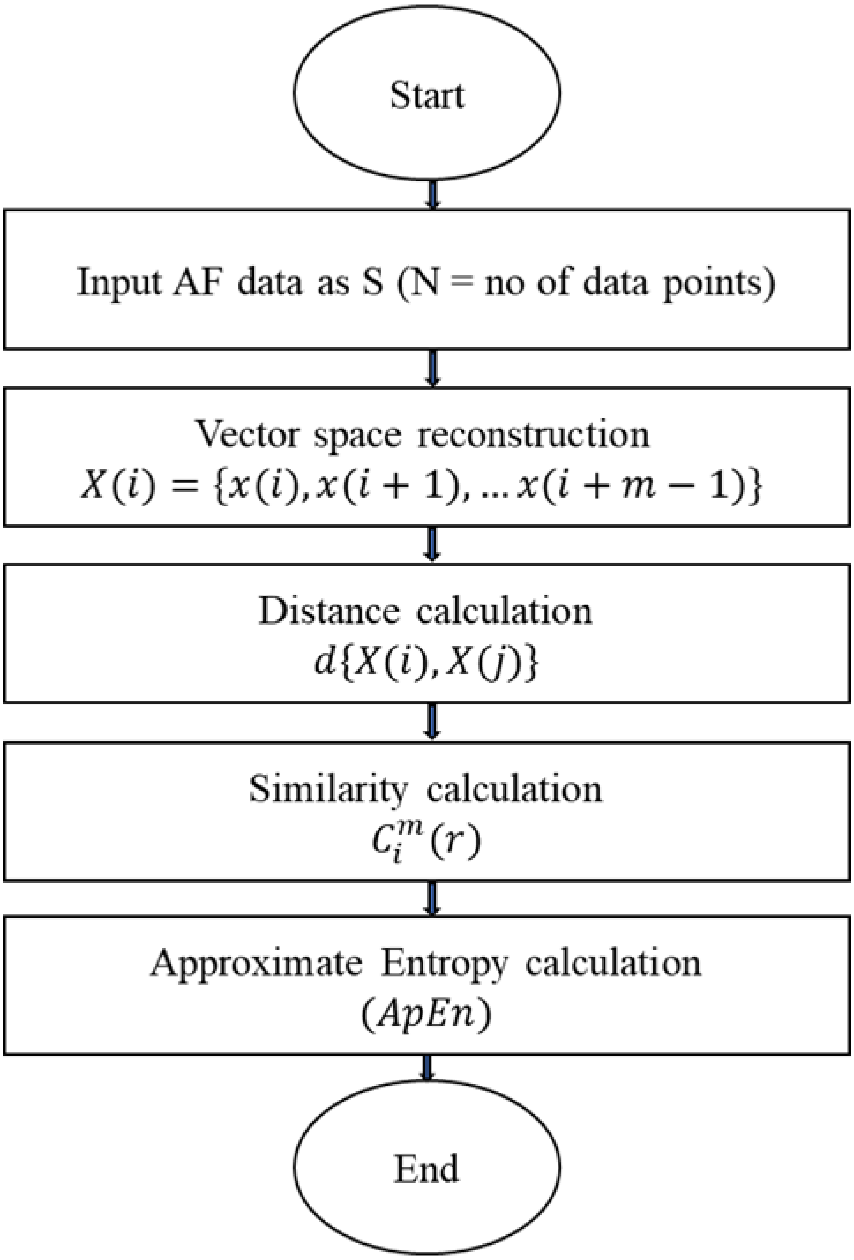

Figure 4. Details algorithm to compute Approximate entropy ($ApEn$) on AF series.

3.5.2. Sample entropy (SampEn)

Sample entropy ($SampEn$) is another modified form of shannon entropy that is used to determine the complexity of physical time series signals and to evaluate physical states. While sample entropy ($SampEn$) is a measure of complexity similar to approximate entropy ($ApEn$), it does not include self-similar patterns [47]. $SampEn$ can be expressed as the negative natural logarithm of the probability that if two sets of simultaneous data points of length m have distance $< r$ then two sets of simultaneous data points of length $m+1$ also have distance $< r$ by equation 9:

$$SampEn(m, r, N) = -\log \frac{A}{B} \tag{9}$$

Where, A = number of template vector pairs having $d(X_{m+1}(i), X_{m+1}(j)) < r$ and B = number of template vector pairs having $d[X_m(i), X_m(j)] < r$, where, m = embedding dimension, r = tolerance, N = number of data points.

Preprints (www.preprints.org) | NOT PEER-REVIEWED | Posted: 12 May 2022 doi:10.20944/preprints202205.0162.v1

3.6. Power spectral density (PSD)

The power spectral density (PSD) is a measurement of the signal's intensity or amplitude's frequency response. In general, it provides a standardized method for describing the distribution of energy in a signal across different frequencies. The PSD of $AF(k)$ as a discrete signal $AF(d)$ can be computed as the average magnitude of the Fourier transform squared [35,48], over a time interval and expressed as equation 10.

$$AF(k) = \left| \frac{1}{2\pi} \sum_{d_1}^{d_2} AF(d) e^{-ikd} \right|^2 = \frac{\widehat{AF}(k)\widehat{AF}_*(k)}{2\pi} \tag{10}$$

where, $\widehat{AF}(k)$ is the discrete Fourier transform of $g(d)$ and $\widehat{AF}_*(k)$ is its complex conjugate, and k is the wave number [35,49–51]. We analyzed this PSD in the power-law domain across the spatial frequency or wave number k as the equation 11.

$$AF(k) \sim \frac{1}{k^{\beta}} \tag{11}$$

where, β is the power-law exponent of the PSD and we referred this β as proxy of planform fluctuations of AF, which is computed using the slope of the linear regression fitted to the estimated PSD plotted on log-log scales [35,52].

4. Results and Discussion

Figure 5a illustrates the yearly pattern of $ApEn$ and $SampEn$, with $ApEn$ having a lower value than $SampEn$. They do, however, follow a similar pattern. The correlation between $SampEn$ and $ApEn$ in figure 5b is linearly positive. While a reasonable correlation was detected with $R^2 \sim= 0.17$, the $t - test$ confirms the correlation's significance with a 95% confidence interval (i.e., $p - value \leq\sim 0.0145$). As illustrated in figures 5a-b, both $ApEn$ and $SampEn$ can be used to quantify the complexity of $AF(d)$; thus, $ApEn$ and $SampEn$ can be referred to as Anastomosing River planform complexity. Although no yearly association with complexity was observed for the 34-year period from 1987 to 2020, we expected that a correlation with river dynamic features may exist. To evaluate the dynamic imprint on river planform complexity, we investigated the correlation between $ApEn$ and $SampEn$ and the yearly maximum discharge (Q_{max}).

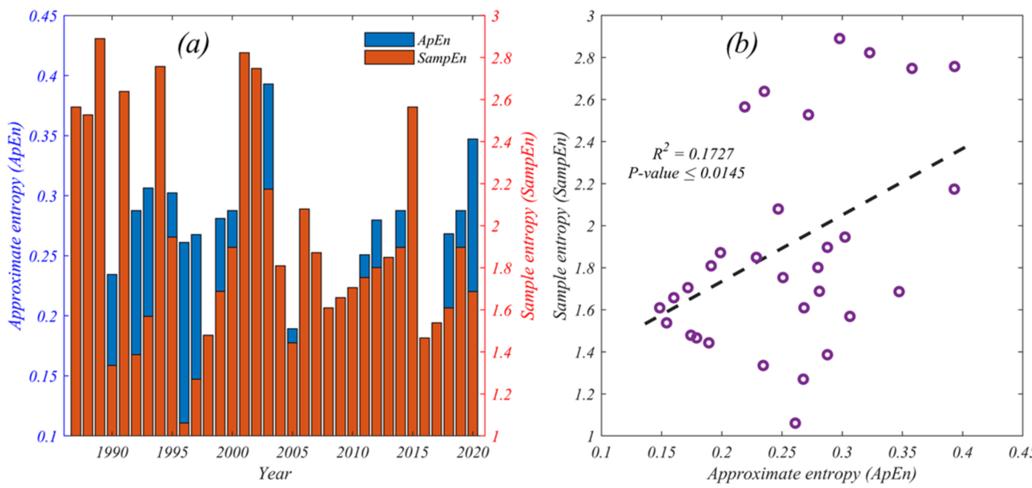

Figure 5. Comparison of Approximate entropy ($ApEn$) and Sample entropy ($SampEn$) on AF series (a) bar plot and (b) linear correlation.

Figure 6a-b exhibits the correlation between Yearly maximum discharge (Q_{max}) with $ApEn$ and $SampEn$. It is observed that, the value of both entropy increases as the Yearly

 doi:10.20944/preprints202205.0162.v1

maximum discharge increases. Hydraulically, higher discharge transports more sediment from the bed and widens the main channel [53], reducing the properties of the Anastomosing River planform and therefore its complexity. On the other hand, reduced discharge deposited more sediments in the river and created a bar, which eventually resulted in oblique flow phenomena, which resulted in a complex network on the Riverine landscape, hence increasing complexity. Apart from physical intuition, both correlations were found to be consistent with the value of $R^2 \sim= 0.06 - 0.07$. Although the $R2$ value is less, the $t - test$ indicates significance correlation within the 95% confidence interval (i.e., $p - value \leq\sim 0.0145$) for $ApEn$ and within the 87% confidence interval (i.e., $p - value \leq\sim 0.126$) for $SampEn$. As a result from our available data, we may conclude that $ApEn$ is a more consistent complexity metric than $SampEn$ to understand Anastomosing River planform.

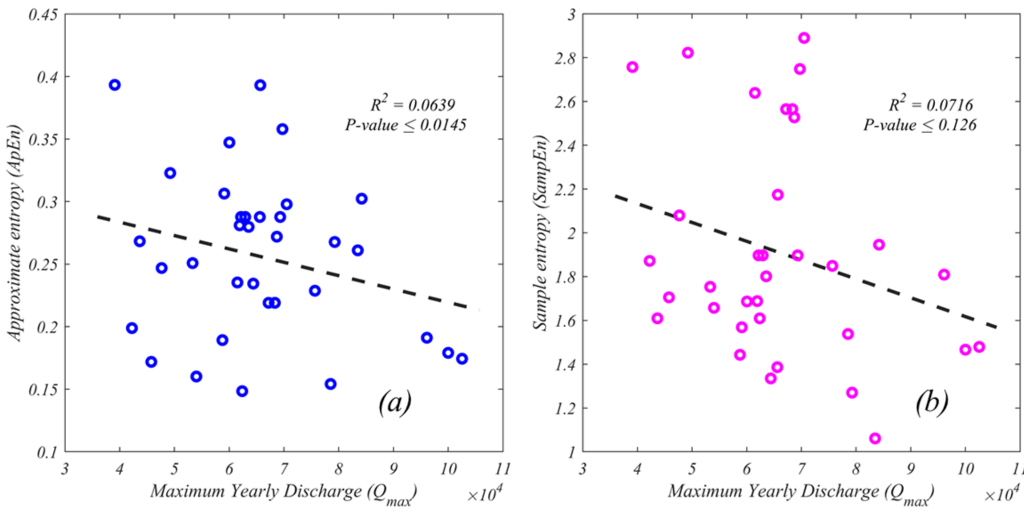

Figure 6. Correlation between (a) Approximate entropy ($ApEn$) and (b) Sample entropy ($SampEn$) with Yearly Maximum discharge (Q_{max}).

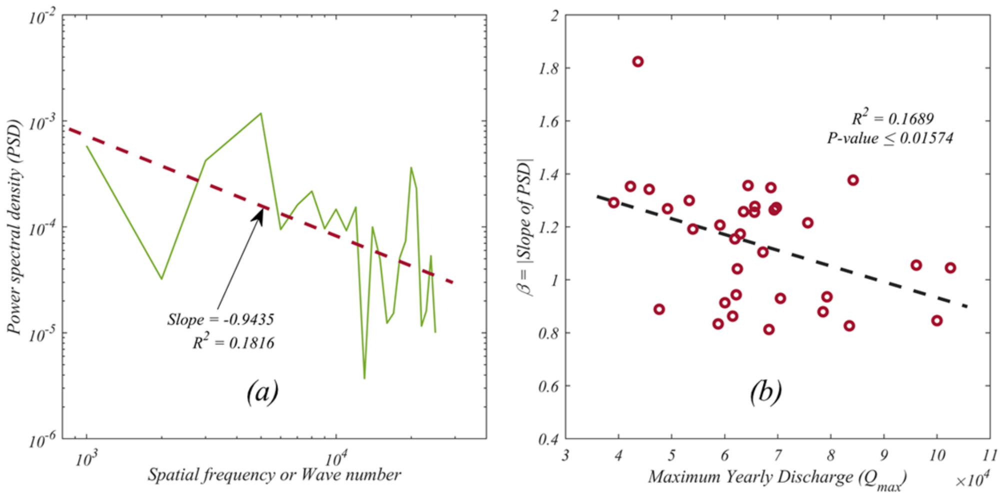

Figure 7. (a) Example of (β) computation using the slope of the linear regression fitted to the estimated PSD plotted on log-log scale and (b) Correlation between (β) with Yearly Maximum discharge (Q_{max}).

The figures 7a-b support our hypothesis that a higher discharge results in less fluctuation on the anastomosing planform and vice versa. In other words, the absolute value of the fitted slope of the PSD of AF plotted on log-log scales can also reflect fluctuation on the anastomosing planform, which is consistent with our complexity results.

5. Concluding Remarks

We have characterized and explored the Brahmaputra River as an anastomosing river in this study, and under this hypothesis, we have proposed a mathematical function called the Anastomosing function AF to characterize the Brahmaputra River's planform. Additionally, we investigate the concept of entropy along with PSD in order to quantify the complexity and fluctuation of planforms. The study's major findings can be summarized as follows:

- The investigated anastomosing function AF is capable of accurately transforming a two-dimensional complex network into a one-dimensional spatial signal.
- The Approximate entropy ($ApEn$) and Sample entropy ($SampEn$) can also be used to quantify the complexity of planforms and reproduced physical features.
- Dynamic imprint such as Yearly Maximum discharge (Q_{max}) has significant contribution on Brahmaputra River and it's planform complexity.
- Yearly Maximum discharge (Q_{max}) has also significant and consistent contribution on Brahmaputra River's planform fluctuation.

Finally, our results reveal the potential to use of Anastomosing function AF along with concept of entropy, PSD and it's characteristics under varying geomorphic, and climatic activities.

Funding: This research received no external funding.

Acknowledgments: The authors would like to thank 'Preprints - The Multidisciplinary Preprint Platform' for accepting our working manuscript.

Conflicts of Interest: The authors declare no conflict of interest.

References

1. Leopold, L.B.; Wolman, M.G. *River channel patterns: braided, meandering, and straight*; US Government Printing Office, 1957.
2. Charlton, R. *Fundamentals of fluvial geomorphology*; Routledge, 2007.
3. Bridge, J.S. The interaction between channel geometry, water flow, sediment transport and deposition in braided rivers. *Geological Society, London, Special Publications* **1993**, *75*, 13–71.
4. Ferguson, R. Understanding braiding processes in gravel-bed rivers: progress and unsolved problems. *Geological Society, London, Special Publications* **1993**, *75*, 73–87.
5. Klaassen, G.J.; Mosselman, E.; Bruehl, H. *On the Prediction of Planform Changes in Braided Sand-nd-Ed Rivers*; Delft Hydraulics, 1993.
6. Pradhan, C.; Chembolu, V.; Bharti, R.; Dutta, S. Regulated rivers in India: research progress and future directions. *ISH Journal of Hydraulic Engineering* **2021**, pp. 1–13.
7. Ashmore, P.E. Laboratory modelling of gravel braided stream morphology. *Earth Surface Processes and Landforms* **1982**, *7*, 201–225.
8. Ashmore, P.E. How do gravel-bed rivers braid? *Canadian journal of earth sciences* **1991**, *28*, 326–341.
9. Ashmore, P. Anabranch confluence kinetics and sedimentation processes in gravel-braided streams. *Geological Society, London, Special Publications* **1993**, *75*, 129–146.
10. Young, W.; Davies, T. Bedload transport processes in a braided gravel-bed river model. *Earth Surface Processes and Landforms* **1991**, *16*, 499–511.
11. Murray, A.B.; Paola, C. A cellular model of braided rivers. *Nature* **1994**, *371*, 54–57.
12. Murray, A.B.; Paola, C. Properties of a cellular braided-stream model. *Earth Surface Processes and Landforms: The Journal of the British Geomorphological Group* **1997**, *22*, 1001–1025.
13. Nykanen, D.K.; Foufoula-Georgiou, E.; Sapozhnikov, V.B. Study of spatial scaling in braided river patterns using synthetic aperture radar imagery. *Water resources research* **1998**, *34*, 1795–1807.
14. Pradhan, C.; Bharti, R.; Dutta, S. Assessment of post-impoundment geomorphic variations along Brahmani River using remote sensing. 2017 IEEE International Geoscience and Remote Sensing Symposium (IGARSS). IEEE, 2017, pp. 5598–5601.
15. Pradhan, C.; Chembolu, V.; Dutta, S. Impact of river interventions on alluvial channel morphology. *ISH Journal of Hydraulic Engineering* **2019**, *25*, 87–93.
16. Sapozhnikov, V.B.; Foufoula-Georgiou, E. Do the current landscape evolution models show self-organized criticality? *Water Resources Research* **1996**, *32*, 1109–1112.
17. Sapozhnikov, V.B.; Foufoula-Georgiou, E. Experimental evidence of dynamic scaling and indications of self-organized criticality in braided rivers. *Water Resources Research* **1997**, *33*, 1983–1991.

18. Walsh, J.; Hicks, D.M. Braided channels: Self-similar or self-affine? *Water Resources Research* **2002**, *38*, 18–1.
19. Lane, S.N.; Westaway, R.M.; Murray Hicks, D. Estimation of erosion and deposition volumes in a large, gravel-bed, braided river using synoptic remote sensing. *Earth Surface Processes and Landforms: The Journal of the British Geomorphological Research Group* **2003**, *28*, 249–271.
20. Westaway, R.; Lane, S.; Hicks, D. The development of an automated correction procedure for digital photogrammetry for the study of wide, shallow, gravel-bed rivers. *Earth Surface Processes and Landforms: The Journal of the British Geomorphological Research Group* **2000**, *25*, 209–226.
21. Westaway, R.M.; Lane, S.N.; Hicks, D.M. Remote sensing of clear-water, shallow, gravel-bed rivers using digital photogrammetry. *Photogrammetric Engineering and Remote Sensing* **2001**, *67*, 1271–1282.
22. Westaway, R.M.; Lane, S.; Hicks, D. Remote survey of large-scale braided, gravel-bed rivers using digital photogrammetry and image analysis. *International Journal of Remote Sensing* **2003**, *24*, 795–815.
23. Coleman, J.M. Brahmaputra River: channel processes and sedimentation. *Sedimentary geology* **1969**, *3*, 129–239.
24. Mosselman, E.; Huisink, M.; Koomen, E.; Seijmonsbergen, A.; others. *Morphological changes in a large braided sand-bed river*; Chichester, EnglandJohn Wiley & Sons, 1995.
25. Thorne, C.R.; Russell, A.P.; Alam, M.K. Planform pattern and channel evolution of the Brahmaputra River, Bangladesh. *Geological Society, London, Special Publications* **1993**, *75*, 257–276.
26. Goswami, D.C. Brahmaputra River, Assam, India: Physiography, basin denudation, and channel aggradation. *Water Resources Research* **1985**, *21*, 959–978.
27. Sarker, S. Essence of MIKE 21C (FDM Numerical Scheme): Application on the River Morphology of Bangladesh. *Open Journal of Modelling and Simulation* **2022**, *10*, 88–117. doi:10.4236/ojmsi.2022.102006.
28. Chembolu, V.; Dutta, S. An entropy based morphological variability assessment of a large braided river. *Earth Surface Processes and Landforms* **2018**, *43*, 2889–2896.
29. Dubey, A.K.; Chembolu, V.; Dutta, S. Utilization of satellite altimetry retrieved river roughness properties in hydraulic flow modelling of braided river system. *International Journal of River Basin Management* **2020**, pp. 1–14.
30. Karmaker, T.; Medhi, H.; Dutta, S. Study of channel instability in the braided Brahmaputra river using satellite imagery. *Current Science* **2017**, pp. 1533–1543.
31. Sarker, M.H.; Thorne, C.R.; Aktar, M.N.; Ferdous, M.R. Morpho-dynamics of the Brahmaputra–Jamuna river, Bangladesh. *Geomorphology* **2014**, *215*, 45–59.
32. Valdiya, K. Why does river Brahmaputra remain untamed? *Current Science* **1999**, *76*, 1301–1305.
33. Dutta, S.; Medhi, H.; Karmaker, T.; Singh, Y.; Prabu, I.; Dutta, U. Probabilistic flood hazard mapping for embankment breaching. *ISH Journal of Hydraulic Engineering* **2010**, *16*, 15–25.
34. Nayak, P.; Panda, B. Brahmaputra and the Socio-Economic Life of People of Assam. *The Mahabahu Brahmaputra, Published by Flood and River Management Agency of Assam, Guwahati, Assam* **2016**, pp. 77–85.
35. Sarker, S. Investigating Topologic and Geometric Properties of Synthetic and Natural River Networks under Changing Climate. *University of Central Florida* **2021**.
36. Sarker, S. Understanding the Complexity and Dynamics of Anastomosing River Planform: A Case Study of Brahmaputra River in Bangladesh. *Earth and Space Science Open Archive* **2021**, p. 1. doi:10.1002/essoar.10508926.2.
37. Sarker, S.; Veremyev, A.; Boginski, V.; Singh, A. Critical nodes in river networks. *Scientific reports* **2019**, *9*, 1–11.
38. Khan, I.; Ahammad, M.; Sarker, S. A study on River Bank Erosion of Jamuna River using GIS and Remote Sensing Technology. *International Journal of Engineering Development and Research* **2014**, *2*, 3365–3371.
39. Marra, W.A.; Kleinhans, M.G.; Addink, E.A. Network concepts to describe channel importance and change in multichannel systems: test results for the Jamuna River, Bangladesh. *Earth Surface Processes and Landforms* **2014**, *39*, 766–778.
40. Makaske, B. Anastomosing rivers: a review of their classification, origin and sedimentary products. *Earth-Science Reviews* **2001**, *53*, 149–196.
41. Ranjbar, S.; Hooshyar, M.; Singh, A.; Wang, D. Quantifying climatic controls on river network branching structure across scales. *Water Resources Research* **2018**, *54*, 7347–7360.
42. Lashermes, B.; Foufoula-Georgiou, E. Area and width functions of river networks: New results on multifractal properties. *Water Resources Research* **2007**, *43*.
43. Shannon, C.E. A mathematical theory of communication. *The Bell system technical journal* **1948**, *27*, 379–423.
44. Delgado-Bonal, A.; Marshak, A. Approximate entropy and sample entropy: A comprehensive tutorial. *Entropy* **2019**, *21*, 541.
45. Pincus, S.M. Approximate entropy as a measure of system complexity. *Proceedings of the National Academy of Sciences* **1991**, *88*, 2297–2301.
46. Pincus, S.; Kalman, R.E. Irregularity, volatility, risk, and financial market time series. *Proceedings of the National Academy of Sciences* **2004**, *101*, 13709–13714.
47. Richman, J.S.; Moorman, J.R. Physiological time-series analysis using approximate entropy and sample entropy. *American Journal of Physiology-Heart and Circulatory Physiology* **2000**.
48. Sarker, S. A Story on the Wave Spectral Properties of Water Hammer. *engrXiv* **July 2021**. doi:https://doi.org/10.31224/osf.io/nhuzq.
49. Stoica, P.; Moses, R.L.; Others. Spectral analysis of signals. *Pearson Prentice Hall Upper Saddle River, NJ* **2005**.
50. Stull, R.B. *An introduction to boundary layer meteorology*; Vol. 13, Springer Science & Business Media, 2012.

51. Gardner, W.A.; Robinson, E.A. Statistical Spectral Analysis—a Nonprobabilistic Theory. *Prentice-Hall, Inc., Division of Simon and Schuster One Lake Street Upper Saddle River, NJUnited States* **1989**.
52. Pilgram, B.; Kaplan, D.T. A comparison of estimators for 1f noise. *Physica D: Nonlinear Phenomena* **1998**, *114*, 108–122.
53. Sarker, S. A Short Review on Computational Hydraulics in the context of Water Resources Engineering. *Open Journal of Modelling and Simulation* **2022**, *10*, 1–31. doi:10.4236/ojmsi.2022.101001.